5338 *Inorg. Chem.* **2009**, *48*, 5338–5349
DOI: 10.1021/ic9003214

Inorganic Chemistry
Article

Synthesis, Structural and Magnetochemical Studies of Iron Phosphonate Cages Based on $\{Fe_3O\}^{7+}$ Core

Sumit Khanra,[†] Sanjit Konar,[‡] Abraham Clearfield,*[,‡] Madeleine Helliwell,[†] Eric J. L. McInnes,[†] Evangelos Tolis,[†] Floriana Tuna,[†] and Richard E. P. Winpenny*[,†]

[†]*School of Chemistry, The University of Manchester, Oxford Road, Manchester M13 9PL, U.K., and* [‡]*Department of Chemistry, Texas A&M University, College Station, Texas 77843*

Received February 19, 2009

We report the synthesis, structures, and magnetic properties of twelve iron(III) phosphonate cages: $[Fe_4(\mu_3\text{-}O)Cl(PhCO_2)_3(PhPO_3)_3(py)_5]$ **1**, $[Fe_4(\mu_3\text{-}O)(^tBuCO_2)_4(C_{10}H_{17}PO_3)_3(py)_4]$ **2** ($C_{10}H_{17}PO_3H_2$ = camphylphosphonic acid), $[Fe_7(\mu_3\text{-}O)_2(PhPO_3)_4(MeCO_2)_9(py)_6]$ **3**, $[Fe_7(\mu_3\text{-}O)_2(PhPO_3)_4(PhCO_2)_9(py)_6]$ **4**, $[Fe_7(\mu_3\text{-}O)_2(^tBuPO_3)_4(^tBuCO_2)_8(py)_8](NO_3)$ **5**, $[Fe_7(\mu_3\text{-}O)_2(PhPO_3)_4(MeCO_2)_8(py)_8]$ **6**, $[Fe_9(\mu_3\text{-}O)_2(\mu_2\text{-}OH)(PhPO_3)_6(^tBuCO_2)_{10}(MeCN)(H_2O)_5]$ **7**, $[Fe_9(\mu_3\text{-}O)_2(\mu_2\text{-}OH)(C_{10}H_{17}PO_3)_6(PhCO_2)_{10}(H_2O)_6]$ **8**, $[Fe_6(\mu_3\text{-}O)_2(O_2)(^tBuCO_2)_8(PhPO_3)_2(H_2O)_2]$ **9**, $[Fe_6(\mu_3\text{-}O)_2(O_2)(^tBuCO_2)_8(C_{10}H_{17}PO_3)_2(H_2O)_2]$ **10**, $[Fe_6(\mu_3\text{-}O)_2(O_2)(^tBuCO_2)_8(^tBuPO_3)_2(py)_2]$ **11**, and $[Fe_{14}(\mu_3\text{-}O)_4(O_2)_2(PhPO_3)_8(^tBuCO_2)_{12}(H_2O)_{12}](NO_3)_2$ **12**. The results have allowed us to compare the magnetic exchange found with magneto-structural correlations found previously for iron-oxo cages.

Introduction

Phosphonates are multidentate ligands that in their mono- or dianionic form can adopt various coordination modes, with a predominance in the literature of 2D- and 3D- framework structures.[1−3] More recently phosphonates have been used to make polymetallic complexes with a range of different nuclearities and shapes.[4−13] One feature of most of these metal phosphonates is the possibility of varying their

*To whom correspondence should be addressed. E-mail: richard.winpenny@manchester.ac.uk. Fax: +44-161-275-4598.

(1) (a) Clearfield, A. *Prog. Inorg. Chem.* **1998**, *47*, 371–510. (b) Poojary, D. M; Zhang, B.; Clearfield, A. *J. Am. Chem. Soc.* **1997**, *119*, 12550–12559. (c) Krishnamohan Sharma, C. V.; Clearfield, A. *J. Am. Chem. Soc.* **2000**, *122*, 4394. (d) Kong, D.; Zoñ, J.; McBee, J.; Clearfield, A. *Inorg. Chem.* **2006**, *45*, 977.

(2) Murugavel, R.; Choudhury, A.; Walawalkar, M. G.; Pothiraja, R.; Rao, C. N. R. *Chem. Rev.* **2008**, *108*, 3549, and refs therein.

(3) (a) Khan, M. I.; Lee, Y. S.; O'Connor, C. J.; Haushalter, R. C.; Zubieta, J. *Inorg. Chem.* **1994**, *33*, 3855. (b) Khan, M. I.; Lee, Y. S.; O'Connor, C. J.; Haushalter, R. C.; Zubieta, J. *Chem. Mater.* **1994**, *6*, 721. (c) Khan, M. I.; Lee, Y. S.; O'Connor, C. J.; Haushalter, R. C.; Zubieta, J. *J. Am. Chem. Soc.* **1994**, *116*, 4525. (d) Finn, R. C.; Zubieta, J.; Haushalter, R. C. *Prog. Inorg. Chem.* **1995**, *51*, 421.

(4) (a) Chandrasekhar, V.; Kingsley, S. *Angew. Chem.* **2000**, *112*, 2410. *Angew. Chem., Int. Ed.* **2000**, *39*, 2320.(b) Chandrasekhar, V.; Nagarajan, L.; Clérac, R.; Ghosh, S.; Verma, S. *Inorg. Chem.* **2008**, *47*, 1067. (c) Chandrasekhar, V.; Sasikumar, P.; Boomishankar, R.; Anantharaman, G. *Inorg. Chem.* **2006**, *45*, 3344. (d) Chandrasekhar, V.; Nagarajan, L.; Clérac, R.; Ghosh, S.; Senapati, T.; Verma, S. *Inorg. Chem.* **2008**, *47*, 5347. (e) Chandrasekhar, V.; Kingsley, S.; Rhatigan, B.; Lam, M. K.; Rheingold, A. L. *Inorg. Chem.* **2002**, *41*, 1030. (f) Chandrasekhar, V.; Sasikumar, P.; Boomishankar, R. *Dalton Trans.* **2008**, 5189. (g) Chandrasekhar, V.; Azhakar, R.; Senapati, T.; Thilagar, P.; Ghosh, S.; Verma, S.; Boomishankar, R.; Steiner, A.; Kogerler, P. *Dalton Trans.* **2008**, 1150. (h) Chandrasekhar, V.; Nagarajan, L.; Gopal, K.; Baskar, V.; Kogerler, P. *Dalton Trans.* **2005**, 3143.

(5) Brechin, E. K.; Coxall, R. A.; Parkin, A.; Parsons, S.; Tasker, P. A.; Winpenny, R. E. P. *Angew. Chem., Int. Ed.* **2001**, *40*, 2700. *Angew. Chem.* **2001**, *113*, 2772.

(6) (a) Tolis, E. I.; Helliwell, M.; Langley, S.; Raftery, J.; Winpenny, R. E. P. *Angew. Chem., Int. Ed.* **2003**, *42*, 3804. (b) Tolis, E. I.; Engelhardt, L. P.; Mason, P. V.; Rajaraman, G.; Kindo, K.; Luban, M.; Matsuo, A.; Nojiri, H.; Raftery, J.; Schroder, C.; Timco, G. A.; Tuna, F.; Wernsdorfer, W.; Winpenny, R. E. P. *Chem.—Eur. J.* **2006**, *12*, 8961–8968. (c) Khanra, S.; Helliwell, M.; Tuna, F.; McInnes, E. J. L.; Winpenny, R. E. P. *Dalton. Trans.* **2009**, in press, doi: b903600h.

(7) (a) Maheswaran, S.; Chastanet, G.; Teat, S. J.; Mallah, T.; Sessoli, R.; Wernsdorfer, W.; Winpenny, R. E. P *Angew. Chem., Int. Ed.* **2005**, *44*, 5044. (b) Shanmugam, M.; Chastanet, G.; Mallah, T.; Sessoli, R.; Teat, S. J.; Timco, G. A.; Winpenny, R. E. P. *Chem.—Eur. J.* **2006**, *12*, 8777. (c) Shanmugam, M.; Shanmugam, M.; Chastanet, G.; Sessoli, R.; Mallah, T.; Wernsdorfer, W.; Winpenny, R. E. P. *J. Mater. Chem.* **2006**, *16*, 2576.

(8) (a) Langley, S.; Helliwell, M.; Sessoli, R.; Teat, S. J; Winpenny, R. E. P. *Inorg. Chem.* **2008**, *47*, 497. (b) Langley, S.; Helliwell, M.; Sessoli, R.; Rosa, P.; Wernsdorfer, W.; Winpenny, R. E. P. *Chem. Commun.* **2005**, *40*, 5029. (c) Langley, S.; Helliwell, M.; Raftery, J.; Tolis, E. I.; Winpenny, R. E. P. *Chem. Commun.* **2004**, *39*, 142. (d) Langley, S.; Helliwell, M.; Sessoli, R.; Teat, S. J.; Winpenny, R. E. P. *Dalton Trans.* **2009**, 3102.

(9) Breeze, B. A.; Shanmugam, M.; Tuna, F.; Winpenny, R. E. P. *Chem. Commun.* **2007**, *42*, 5185.

(10) (a) Khanra, S.; Kloth, M.; Mansaray, H.; Muryn, C. A.; Tuna, F.; Sañudo, E. C.; Helliwell, M.; McInnes, E. J. L.; Winpenny, R. E. P. *Angew. Chem., Int. Ed.* **2007**, *46*, 5568. (b) Khanra, S.; Helliwell, M.; Tuna, F.; McInnes, E. J. L.; Winpenny, R. E. P. *J. Mol. Struct.* **2008**, *890*, 157.

(11) (a) Konar, S.; Bhuvanesh, N.; Clearfield, A. *J. Am. Chem. Soc.* **2006**, *128*, 9604. (b) Konar, S.; Clearfield, A. *Inorg. Chem.* **2008**, *47*, 5573. (c) Konar, S.; Clearfield, A. *Inorg. Chem.* **2008**, *47*, 3492. (d) Konar, S.; Clearfield, A. *Inorg. Chem.* **2008**, *47*, 3489.

(12) (a) Walawalkar, M. G.; Murugavel, R.; Voigt, A.; Roesky, H. W.; Schmidt, H.-G. *J. Am. Chem. Soc.* **1997**, *119*, 4656. (b) Walawalkar, M. G.; Horchler, S.; Dietrich, S.; Chakraborty, D.; Roesky, H. W.; Schafer, M.; Schmidt, H.-G.; Sheldrick, G. M.; Murugavel, R. *Organometallics.* **1998**, *17*, 2865. (c) Walawalkar, M. G.; Murugavel, R.; Roesky, H. W.; Uson, I.; Kraetzner, R. *Inorg. Chem.* **1998**, *37*, 473. (d) Murugavel, R.; Shanmugan, S. *Chem. Commun.* **2007**, 1257.

(13) (a) Yang, Y.-F.; Ma, Y.-S.; Guo, L.-R.; Zheng, L.-M. *Cryst. Growth. Des.* **2008**, *8*, 1213. (b) Hou, J.-J.; Zhang, X.-M. *Cryst. Growth. Des.* **2006**, *6*, 1445. (c) Ma, Y.-S.; Song, Y.; Li, Y.-Z.; Zheng, L.-M. *Inorg. Chem.* **2007**, *46*, 5459. (d) Du, Z.-Y.; Prosvirin, A. V.; Mao, J.-G. *Inorg. Chem.* **2007**, *46*, 9884. (e) Ma, Y.-S.; Li, Y.-Z.; Song, Y.; Zheng, L.-M. *Inorg. Chem.* **2008**, *47*, 4536.

Published on Web 05/11/2009

structures and properties by changing the nature of the alkyl or the aryl group attached to the phosphorus.

Three approaches to the synthesis of metal-phosphonate cages are currently being exploited. The first arises from an initial report by Chandrasekhar and Kingsley,[4a] where a second ligand is added alongside the phosphonate to prevent formation of an insoluble polymer. We have used this with pyridonates and carboxylates as co-ligands, and produced cobalt,[5,8] nickel[9] and vanadium (III) cages[10] as a result. The second approach is to react phosphonates with preformed metal carboxylate triangles, which was originally reported for manganese[5,7] and later for iron(III)[6] and has since been extended.[11,13] The third approach which is similar to the approach used to make 2D- and 3D- materials was pioneered for phosphonate cages by Zubieta.[3] This approach uses solvothermal techniques to overcome the insolubility of the compounds, and has produced cages with the higher oxidation states of vanadium.

The magnetic properties of these phosphonate cages can be interesting. Some of the manganese cages are single molecule magnets, for example, a cage with a $\{Mn^{III}_{18}Mn^{II}_{2}\}$ core has an energy barrier of 43 K,[7a] while a $\{Co^{II}_{8}\}$ cage appears to be an unusual single-chain magnet.[8a] An $\{Fe_9\}$ cage shows a fairly large phonon bottleneck leading to non-monotonic behavior of the magnetization at lowest temperatures.[6b]

We report here the synthesis, structures, and magnetic properties of twelve iron(III) phosphonate cages: $[Fe_4(\mu_3\text{-}O)Cl(PhCO_2)_3(PhPO_3)_3(py)_5]$ **1**, $[Fe_4(\mu_3\text{-}O)(^tBuCO_2)_4(C_{10}H_{17}PO_3)_3(py)_4]$ **2** ($C_{10}H_{17}PO_3H_2$ = camphylphosphonic acid), $[Fe_7(\mu_3\text{-}O)_2(PhPO_3)_4(MeCO_2)_9(py)_6]$ **3**, $[Fe_7(\mu_3\text{-}O)_2(PhPO_3)_4(PhCO_2)_9(py)_6]$ **4**, $[Fe_7(\mu_3\text{-}O)_2(^tBuPO_3)_4(^tBuCO_2)_8(py)_8](NO_3)$ **5**, $[Fe_7(\mu_3\text{-}O)_2(PhPO_3)_4(MeCO_2)_8(py)_8]$ **6**, $[Fe_9(\mu_3\text{-}O)_2(\mu_2\text{-}OH)(PhPO_3)_6(^tBuCO_2)_{10}(MeCN)(H_2O)_5]$ **7**, $[Fe_9(\mu_3\text{-}O)_2(\mu_2\text{-}OH)(C_{10}H_{17}PO_3)_6(PhCO_2)_{10}(H_2O)_6]$ **8**, $[Fe_6(\mu_3\text{-}O)_2(O_2)(^tBuCO_2)_8(PhPO_3)_2(H_2O)_2]$ **9**, $[Fe_6(\mu_3\text{-}O)_2(O_2)(^tBuCO_2)_8(C_{10}H_{17}PO_3)_2(H_2O)_2]$ **10**, $[Fe_6(\mu_3\text{-}O)_2(O_2)(^tBuCO_2)_8(^tBuPO_3)_2(py)_2]$ **11**, and $[Fe_{14}(\mu_3\text{-}O)_4(O_2)_2(PhPO_3)_8(^tBuCO_2)_{12}(H_2O)_{12}](NO_3)_2$ **12**. The results have allowed us to compare the magnetic exchange found with magneto-structural correlations proposed previously for iron-oxo cages.[14a,15] Many previous examples of iron-oxo cages exist, with perhaps the earliest significant work published from the Lippard group and involving carboxylate ligands.[14] This early work has been reviewed.[16]

Experimental Section

Synthesis. Starting Materials. All preparations were performed under aerobic conditions using reagents and solvents as received. $[Fe_3(\mu_3\text{-}O)(PhCO_2)_6(H_2O)_3]Cl$, $[Fe_3(\mu_3\text{-}O)(MeCO_2)_6(H_2O)_3]Cl$, $[Fe_3(\mu_3\text{-}O)(^tBuCO_2)_6(H_2O)_3]Cl$, and $[Fe_3(\mu_3\text{-}O)(^tBuCO_2)_6(H_2O)_3](NO_3)$ were synthesized according to literature procedures.[17] Camphyl phosphonic acid ($C_{10}H_{17}PO_3H_2$) was obtained from the Donjindo Chemical Company, Japan.

$[Fe_4(\mu_3\text{-}O)Cl(PhCO_2)_3(PhPO_3)_3(py)_5]$ 1. $[Fe_3(\mu_3\text{-}O)(PhCO_2)_6(H_2O)_3]Cl$ (0.5 g, 0.5 mmol) and $PhPO_3H_2$ (0.158 g, 1.00 mmol) were added to pyridine (10 mL), and the reaction mixture was stirred for 24 h. The solution was filtered, and Et_2O was allowed to diffuse into the red filtrate. This gave crystals of **1**. Yield: 0.19 g (51.1% based on Fe) Elemental analysis calcd (%) for $\mathbf{1}\cdot H_2O$ ($C_{64}H_{57}Fe_4N_5O_{17}ClP_3$): C 50.57, H 3.78, N 4.61, Cl 2.33, Fe 14.70, P 6.11; found: C 50.70, H 3.71, N 4.49, Cl 2.49, Fe 14.77, P 5.80.

$[Fe_4(\mu_3\text{-}O)(^tBuCO_2)_4(C_{10}H_{17}PO_3)_3(py)_4]$ 2. $[Fe_3(\mu_3\text{-}O)(^tBuCO_2)_6(H_2O)_3]Cl$ (88 mg, 0.1 mmol), $C_{10}H_{17}PO_3H_2$ (22 mg, 0.10 mmol), and pyridine (0.50 mL, 6 mmol) were added to CH_3CN (5 mL), and the solution stirred overnight. The greenish red solution was filtered, and Et_2O (5 mL) added before the solution was allowed to evaporate slowly at 4 °C. After 2−3 days large orange crystals were collected for single-crystal X-ray analysis. Yield: 0.086 g (54% based on Fe). Elemental analysis calcd (%) for **2** ($C_{70}H_{107}Fe_4N_4O_{18}P_3$): C 52.26, H 6.70, N 3.48, Fe 13.88, P 5.78; found: C 52.53, H 6.65, N 3.45, Fe 13.69, P 5.86.

$[Fe_7(\mu_3\text{-}O)_2(MeCO_2)_9(PhPO_3)_4(py)_6]$ 3. $[Fe_3(\mu_3\text{-}O)(MeCO_2)_6(H_2O)_3](NO_3)$ (0.32 g, 0.5 mmol), pyridine (0.24 mL, 3.0 mmol), and $PhPO_3H_2$ (0.19 g, 1.0 mmol) were added to $MeNO_2$ (10 mL), and the mixture stirred for 5 h, then filtered. Et_2O was allowed to diffuse into the red filtrate giving crystals after 5−6 days suitable for X-ray analysis. Yield: 0.11 g (21.6% based on Fe). Elemental analysis (%): calcd for $\mathbf{3}\cdot 3CH_3NO_2$ ($C_{75}H_{86}Fe_7N_9O_{38}P_4$): C 40.28, H 3.88; N 5.64; Fe 17.48, P 5.54, found: C 40.35, H 3.71, N 5.68, Fe 17.32, P 5.39.

$[Fe_7(\mu_3\text{-}O)_2(PhCO_2)_9(PhPO_3)_4(py)_6]$ 4. $[Fe_3(\mu_3\text{-}O)(PhCO_2)_6(H_2O)_3](Cl)$ (0.5 g, 0.5 mmol), pyridine (0.24 mL, 3.0 mmol), and $PhPO_3H_2$ (0.158 g, 1.0 mmol) were added to 1:1 CH_3CN/CH_2Cl_2 as the solvent (10 mL), and the mixture stirred for 5 h, then filtered. Et_2O was allowed to diffuse into the red filtrate giving crystals after 3 days suitable for X-ray analysis. Yield: 0.115 g (17.35% based on Fe). Elemental analysis calcd (%) for $\mathbf{4}\cdot CH_2Cl_2$ ($C_{118}H_{97}Fe_7N_6O_{32}Cl_2P_4$): C 52.55, H 3.63, N 3.12, Fe 14.5, P 4.6, Cl 2.63; found: C 52.34, H 3.60, N 3.15, Fe 14.55, P 4.5, Cl 2.66.

$[Fe_7(\mu_3\text{-}O)_2(^tBuCO_2)_8(^tBuPO_3)_4(py)_8](NO_3)$ 5. $[Fe_3(\mu_3\text{-}O)(^tBuCO_2)_6(H_2O)_3](NO_3)$ (0.27 g, 0.3 mmol), pyridine (0.14 mL, 1.8 mmol), and $^tBuPO_3H_2$ (0.083 g, 0.6 mmol) were added to CH_3CN as the solvent (10 mL), and the mixture stirred for 5 h, then filtered. Et_2O was allowed to diffuse into the red filtrate giving crystals after 7 days suitable for X-ray analysis. Yield: 0.104 g (ca. 30% based on Fe). Elemental analysis calcd (%) for **5** ($C_{96}H_{148}Fe_7N_9O_{33}P_4$): C 46.66, H 6.04, N 5.10, Fe 15.83, P 5.01; found: C 46.34, H 5.90, N 5.08, Fe 15.55, P 4.85.

$[Fe_7(\mu_3\text{-}O)_2(MeCO_2)_8(PhPO_3)_4(py)_8]$ 6. $[Fe_3(\mu_3\text{-}O)(MeCO_2)_6(H_2O)_3](Cl)$ (0.19 g, 0.3 mmol), pyridine (0.14 mL, 1.8 mmol), and $PhPO_3H_2$ (0.095 g, 0.6 mmol) were added to CH_3CN (10 mL), and the mixture stirred for 5 h, then filtered. Et_2O was allowed to diffuse into the red filtrate giving crystals after 7 days suitable for X-ray analysis. Yield: 0.055 g (19.3% based on Fe). Elemental analysis calcd (%) for **6** ($C_{80}H_{84}Fe_7N_8O_{30}P_4$): C 44.64, H 3.93, N 5.21, Fe 18.16, P 5.76; found: C 44.94, H 3.80, N 5.18, Fe 18.05, P 5.53.

$[Fe_9(\mu_3\text{-}O)_2(\mu_2\text{-}OH)(^tBuCO_2)_{10}(PhPO_3)_6(H_2O)_5(MeCN)]$ 7. $[Fe_3(\mu_3\text{-}O)(^tBuCO_2)_6(H_2O)_3]Cl$ (0.176 g, 0.20 mmol) and $PhPO_3H_2$ (0.0316 g, 0.2 mmol) were added to CH_3CN (5 mL), and the solution stirred overnight. The yellow-orange solution was filtered, and Et_2O (5 mL) added before the solution was allowed to evaporate slowly at 4 °C. Yellowish-orange crystals were collected after few days. Yield: 0.07 g (33.7% based on Fe). Elemental analysis calcd (%) for **7** ($C_{88}H_{134}Fe_9N_1O_{46}P_6$): C 40.18, H 5.14, N 0.53, Fe 19.11, P 7.07; found: C 39.96, H 5.02, N 0.57, Fe 18.93, P 6.90.

(14) (a) Gorun, S. M.; Lippard, S. *J. Inorg. Chem* **1991**, *30*, 1625. (b) Micklitz, W.; Bott, S. G.; Bentsen, J. G.; Lippard, S. J. *J. Am. Chem. Soc*. **1989**, *111*, 372. (c) Micklitz, W.; Lippard, S. J. *J. Am. Chem. Soc*. **1989**, *111*, 6856. Gorun, S. M.; Lippard, S. J. *Nature* **1986**, *319*, 666.

(15) (a) Weihe, H.; Gudel, H. U. *J. Am. Chem. Soc*. **1997**, *119*, 6539. (b) Canada-Vilalta, C.; O'Brien, T. A.; Brechin, E. K.; Pink, M.; Davidson, E. R.; Christou, G. *Inorg. Chem*. **2004**, *43*, 5505.

(16) (a) Gatteschi, D.; Caneschi, A.; Sessoli, R.; Cornia, A. *Chem. Soc. Rev*. **1996**, *25*, 101. (b) Gatteschi, D.; Sessoli, R.; Cornia, A. *Chem. Commun*. **2000**, 725.

(17) (a) Wilson, C.; Iversen, B. B.; Overgaard, J.; Larsen, F. K.; Wu, G.; Palii, S. P.; Timco, G. A.; Gerbeleu, N. V. *J. Am. Chem. Soc*. **2000**, *122*, 11370. (b) Batsanov, A. S.; Struchkov, Yu. T.; Timko, G. A. *Koord. Khim*. **1988**, *14*, 266.

$[Fe_9(\mu_3\text{-}O)_2(\mu_2\text{-}OH)(PhCO_2)_{10}(C_{10}H_{17}PO_3)_6(H_2O)_6]$ 8. $[Fe_3(\mu_3\text{-}O)(PhCO_2)_6(H_2O)_3]Cl$ (99 mg, 0.10 mmol) and camphyl phosphonic acid (22 mg, 0.1 mmol) were added to CH_3CN (5 mL), and the solution stirred overnight. The yellow-orange solution was filtered, and Et_2O (5 mL) added before the solution was allowed to evaporate slowly at 4 °C. Yellowish-orange crystals were collected after few days. The yield of the reaction: 0.055 g (ca. 46% based on Fe). Elemental analysis calcd (%) for **8** ($C_{130}H_{165}Fe_9O_{47}P_6$): C 49.28, H 5.24, Fe 15.86, P 5.87; found: C 49.07, H 5.08, Fe 15.55, P 5.70.

$[Fe_6(\mu_3\text{-}O)_2(O_2)(^tBuCO_2)_8(PhPO_3)_2(H_2O)_2]$ 9. $[Fe_3(\mu_3\text{-}O)(^tBuCO_2)_6(H_2O)_3](NO_3)$ (0.47 g, 0.5 mmol) and $PhPO_3H_2$ (0.079 g, 0.5 mmol) were added to CH_3CN (7 mL), and 2 drops of H_2O_2 (30% in H_2O) were added. The solution stirred for 1 h after which it turned red. Then the solution was allowed to stand undisturbed at 4 °C for few days. Dark red crystals suitable for X-ray analysis formed. Yield: 0.21 g (42% based on Fe) Elemental analysis calcd (%) for **9**·MeCN ($C_{54}H_{89}Fe_6O_{28}P_2N_1$): C 40.60, H 5.62, N 0.88, Fe 20.98, P 3.88; found: C 40.17, H 5.53, N 0.79, Fe 20.67, P 3.84.

$[Fe_6(\mu_3\text{-}O)_2(O_2)(^tBuCO_2)_8(C_{10}H_{17}PO_3)_2(H_2O)_2]$ 10. $[Fe_3(\mu_3\text{-}O)(^tBuCO_2)_6(H_2O)_3](NO_3)$ (90 mg, 0.1 mmol) and camphyl phosphonic acid (22.mg, 0.1 mmol) were added to CH_3CN (5 mL), and 1 drop of H_2O_2 (30% in H_2O) was added. The solution stirred overnight. The intense red solution was filtered and allowed to evaporate slowly at 4 °C. After 2−3 days large crystals were collected for single-crystal X-ray analysis. Yield: 0.039 g (35% based on Fe). Elemental analysis calcd (%) for **10** ($C_{60}H_{110}Fe_6O_{28}P_2$): C 42.98, H 6.61, Fe 19.99, P 3.70; found: C 42.71, H 6.49, Fe 19.54, P 3.52.

$[Fe_6(\mu_3\text{-}O)_2(O_2)(^tBuCO_2)_8(^tBuPO_3)_2(py)_2]$ 11. $[Fe_3(\mu_3\text{-}O)(^tBuCO_2)_6(H_2O)_3](NO_3)$(0.27 g, 0.3 mmol), $^tBuPO_3H_2$ (0.041 g, 0.3 mmol) were added to CH_3CN (7 mL), and 2 drops of H_2O_2 (30% in H_2O) and 3−4 drops of py were added. The solution stirred for 4 h after which it turned red. Then the solution was allowed to stand undisturbed at 4 °C for few days. Dark red crystals suitable for X-ray analysis formed after 3−4 days. Yield: 0.095 g (30.5% based on Fe) Elemental analysis calcd (%) for **11** ($C_{58}H_{100}Fe_6N_2O_{26}P_2$): C 42.52, H 6.15, N 1.71, Fe 20.45, P 3.78; found: C 42.68, H 6.11, N 1.63, Fe 20.26 P 3.67.

$[Fe_{14}(\mu_3\text{-}O)_4(O_2)_2(^tBuCO_2)_{12}(PhPO_3)_8(H_2O)_{12}](NO_3)_2$ 12. $[Fe_3(\mu_3\text{-}O)(^tBuCO_2)_6(H_2O)_3](NO_3)$ (0.27 g, 0.3 mmol) and $PhPO_3H_2$ (0.047 g, 0.3 mmol) were added to CH_3CN (7 mL), and the solution was stirred overnight. The solution was filtered, and Et_2O (10 mL) added before the solution was allowed to evaporate slowly. Yield: 0.046 g (14.5% based on Fe). Elemental analysis (%): calcd for **12** ($C_{108}H_{172}Fe_{14}N_2O_{74}P_8$): C 34.94, H 4.67, N 0.75, Fe 21.06, P6.68; found: C 34.65, H 4.59, N 0.64, Fe 20.78, P6.52.

X-ray Crystallographic Data Collection and Refinement of the Structures. Data for **1**, **2**, **3**, **4**, **8**, **10**, and **12** were collected on a Bruker SMART CCD diffractometer; data for **5**−**7** and **11** were collected on an Oxford Instruments CCD diffractometer (both Mo Kα, λ = 0.71069 Å). Crystal data and refinement parameters are given in Table 1. In all cases the selected crystals were mounted on the tip of a glass pin using Paratone-N oil and placed in the cold flow (120 K) produced with an Oxford Cryocooling device. Complete hemispheres of data were collected using ω scans (0.3°, 30−50 s/frame). Integrated intensities were obtained with SAINT+, and they were corrected for absorption using SADABS. Structure solution and refinement was performed with the SHELX package.[18] The structures were solved by direct methods and completed by iterative cycles of ΔF syntheses and full-matrix least-squares refinement against F^2. Crystal data for **1**−**4**, **8**−**10**, and **12** have been described previously,[6a,11a] and CIF files are available from the Cambridge Crystallographic Data Centre with CCDC numbers and codes: **1** 208770 (EKUROR), **2** 621915 (CEPFAF), **3** 208771 (EKURUX), **4** 208772 (EKUSAE), **8** 621913(CEPDOR), **9** 208775 (EKUSOS), **10** 621914 (CEPDUX), **12** 208774 (EKUSIM).

Magnetic Measurements. Magnetic susceptibility and magnetization measurements were performed on polycrystalline samples restrained in eicosane, using a Quantum Design MPMS XL SQUID magnetometer equipped with a 7 T magnet. Data were corrected for the diamagnetism of the compounds by using Pascal constants and for the diamagnetic contributions of the sample holder and eicosane by measurement. The magnetic susceptibilities of the compounds were collected in the temperature range 2−300 K with an applied magnetic field of 0.1 T. Simulation of magnetic data used MAGPACK.[19]

Results and Discussion

Synthesis. Many synthetic procedures to polynuclear iron clusters rely on the reaction of $[Fe_3(\mu_3\text{-}O)(RCO_2)_6(L)_3]X$ (R = Me, Ph, ^{t}Bu; X = Cl, NO_3) species with a potentially chelating or bridging ligand, and this was one of the procedures chosen in the present work. In such reactions, the $\{Fe_3(\mu_3\text{-}O)\}^{7+}$ core serves as a building block for high nuclearity clusters, but the exact nuclearity and structure of the product depend on several factors; in the present work, we have found the influence of solvents, carboxylate co-ligands, bases, and X group. We have been able to make similar cages with different phosphonates—phenyl, camphyl, or *t*-butyl—which suggests the organic substituent on the phosphonate ligand is not as important as the reaction conditions.

The reaction of $[Fe_3(\mu_3\text{-}O)(PhCO_2)_6(H_2O)_3]Cl$ with 2 equiv of $PhPO_3H_2$ in pyridine gave a red solution from which a tetranuclear iron cage $[Fe_4(\mu_3\text{-}O)Cl(PhCO_2)_3(PhPO_3)_3(py)_5]$ **1** was obtained by diffusing Et_2O into the filtrate. The formulation of **1** is summarized in eq 1:

$$4[Fe_3(\mu_3{-}O)(PhCO_2)_6(H_2O)_3]Cl + 9PhPO_3H_2 + 15py \rightarrow 3[Fe_4(\mu_3{-}O)Cl(PhCO_2)_3(PhPO_3)_3(py)_5] + 15PhCO_2H + HCl + H_2O \quad (1)$$

A similar tetranuclear cage $[Fe_4(\mu_3\text{-}O)(^tBuCO_2)_4(C_{10}H_{17}PO_3)_3(py)_4]$ **2** can also be made from reaction between $[Fe_3(\mu_3\text{-}O)(^tBuCO_2)_6(H_2O)_3]Cl$ and $C_{10}H_{17}PO_3H_2$ in MeCN with excess pyridine present; the core of the cage is the same in **1** and **2** but the peripheral ligands are different. The formation of **2** can be summarized in eq 2:

$$4[Fe_3(\mu_3{-}O)(^tBuCO_2)_6(H_2O)_3]Cl + 9C_{10}H_{17}PO_3H_2 + 12py \rightarrow 3[Fe_4(\mu_3{-}O)(^tBuCO_2)_4(C_{10}H_{17}PO_3)_3(py)_4] + 12\,^tBuCO_2H + 4HCl + H_2O \quad (2)$$

If the amount of pyridine used is reduced a family of heptanuclear cages can be made in solvents such as $MeNO_2$, CH_3CN or 1:1 CH_3CN-CH_2Cl_2. Treatment of $[Fe_3(\mu_3\text{-}O)(MeCO_2)_6(H_2O)_3]Cl$ with 2 equiv of $PhPO_3H_2$ and pyridine as a base gave an orange red solution from which $[Fe_7(\mu_3\text{-}O)_2(MeCO_2)_9(PhPO_3)_4(py)_6]$ **3** and $[Fe_7(\mu_3\text{-}O)_2(MeCO_2)_8(PhPO_3)_4(py)_8]$ **6** were subsequently isolated by diffusion of Et_2O into $MeNO_2$ (for **3**) or MeCN

(18) *SHELX-PC Package*; Bruker Analytical X-ray Systems: Madison, WI, **1998**.

(19) Borrás-Almenar, J. J.; Clemente-Juan, J. M.; Coronado, E.; Tsukerblat, B. S. *J. Comput. Chem.* **2001**, *22*, 985.

Table 1. Crystal Data and Refinement Parameters for Compounds **1**−**12**

compound	**1**	**2**	**3**	**4**
formula	$C_{87}H_{70}ClFe_4N_8O_{18}P_3$	$C_{78}H_{119}Fe_4N_8O_{18}P_3$	$C_{72}H_{64}Fe_7N_6O_{32}P_4$	$C_{119}H_{98}Fe_7N_7O_{32}P_4$
M	5601.81	1771.27	2040.12	2652.88
cryst syst	rhombohedral	monoclinic	triclinic	orthorhombic
space group	$R3$	$P2_1/c$	$P\bar{1}$	$Pca2_1$
a/Å	41.1922(18)	21.865(16)	16.104(2)	27.865(3)
b/Å	41.1922(18)	19.796(15)	19.212(2)	20.534(2)
c/Å	29.1310(17)	20.370(15)	20.976(3)	20.583(3)
α/deg	90	90	66.906(2)	90
β/deg	90	92.539(10)	72.105(2)	90
α/deg	120	90	87.153(2)	90
U/Å^3	42807(3)	8808(11)	5662.4(12)	11777(2)
T/K	100(2)	100(2)	100(2)	100(2)
Z	18	4	2	4
μ/mm^{-1}	1.304	2.032	1.197	1.496
unique data	22991	13064	24767	22844
data with $F_o > 4\sigma(F_o)$	14467	7285	7773	17174
R1, wR2[a]	0.0579, 0.2018	0.1045, 0.3175	0.1293, 0.4381	0.0530, 0.1194
compound	**5**	**6**	**7**	**8**
formula	$C_{118.5}H_{170.5}Fe_7N_{13.5}O_{33}P_4$	$C_{117.5}H_{121.5}Fe_7N_{15.5}O_{30}P_4$	$C_{97}H_{148.5}Fe_9N_{5.5}O_{46.5}P_6$	$C_{146}H_{177}Fe_9N_8O_{47}P_6$
M	2827.01	2745.63	2824.18	3484.43
cryst syst	monoclinic	monoclinic	monoclinic	triclinic
space group	$C2/m$	$P2_1/c$	$P2_1/n$	$P\bar{1}$
a/Å	22.667 (5)	27.2371(19)	15.7176(6)	17.242(3)
b/Å	16.973(5)	18.5032(14)	31.6232(12)	17.966(3)
c/Å	21.914(5)	33.210(3)	27.2512(12)	31.315(5)
α/deg	90	90	90	88.324(3)
β/deg	110.499(5)	125.111(6)	98.365(4)	75.316(3)
α/deg	90	90	90	86.238(3)
U/Å^3	7897(3)	13691.5 (19)	13400.9(9)	9363(3)
T/K	100(2)	100(2)	100(2)	100(2)
Z	2	4	4	2
μ/mm^{-1}	1.189	1.332	1.400	1.236
unique data	14879	14293	52533	56808
data with $F_o > 4\sigma(F_o)$	4288	4365	16421	32144
R1, wR2[a]	0.1086, 0.3134	0.0824, 0.2038	0.0688, 0.1642	0.1193, 0.3470
compound	**9**	**10**	**11**	**12**
formula	$C_{56}H_{92}Fe_6N_2O_{28}P_2$	$C_{65.1}H_{113.65}Fe_6N_{2.55}O_{28}P_2$	$C_{59.5}H_{102.25}Fe_6N_{2.75}O_{26}P_2$	$C_{120}H_{130}Fe_{14}N_8O_{82}P_8$
M	1638.36	1777.18	1669.23	4025.96
cryst syst	orthorhombic	monoclinic	monoclinic	orthorhombic
space group	$Pnma$	$P2_1/n$	$P2_1/n$	$Pnn2$
a/Å	17.0228(15)	16.0253(18)	14.9882(8)	23.3688(19)
b/Å	18.6228(17)	23.845(3)	23.7909(12)	26.584(2)
c/Å	22.836(2)	24.665(3)	24.8382(12)	15.2904(12)
α/deg	90	90	90	90
β/deg	90	100.269(2)	98.135(5)	90
α/deg	90	90	90	90
U/Å^3	7239.3(11)	9274.1(4)	8767.8(8)	9499.0(13)
T/K	100(2)	100(2)	100(2)	100(2)
Z	4	4	4	2
μ/mm^{-1}	1.503	1.273	1.265	1.408
unique data	7661	55939	43785	19287
data with $F_o > 4\sigma(F_o)$	7010	20794	11238	16810
R1, wR2[a]	0.0269, 0.0740	0.0854, 0.2344	0.0693, 0.1856	0.0599, 0.1804

[a] R1 reported for data with $F_o > 4\sigma(F_o)$, wR2 reported for all data.

(for **6**). Similarly the reaction of $[Fe_3(\mu_3\text{-}O)(PhCO_2)_6(H_2O)_3]Cl$ instead of using $[Fe_3(\mu_3\text{-}O)(MeCO_2)_6(H_2O)_3]Cl$ gave a similar corresponding heptanuclear cluster $[Fe_7(\mu_3\text{-}O)_2(PhCO_2)_9(PhPO_3)_4(py)_6]$ **4**. The formulation of the heptanuclear clusters **3** and **4** can be summarized as

$$7[Fe_3(\mu_3{-}O)(RCO_2)_6(H_2O)_3]Cl + 12PhPO_3H_2 + 18py \rightarrow 3[Fe_7(\mu_3{-}O)_2(RCO_2)_9(PhPO_3)_4(py)_6] + 15RCO_2H + 7HCl + H_2O \quad (R = Me, Ph) \quad (3)$$

If the carboxylate employed was pivalate instead of acetate or benzoate, the product from the $[Fe_3(\mu_3\text{-}O)(^tBuCO_2)_6(H_2O)_3]NO_3$ reaction with $^tBuPO_3H_2$ in MeCN was another heptanuclear complex $[Fe_7(\mu_3\text{-}O)_2(^tBuCO_2)_8(^tBuPO_3)_4(Py)_8](NO_3)$ **5**. The formation of **5** and **6** can be summarized as

$$7[Fe_3(\mu_3{-}O)(RCO_2)_6(H_2O)_3]X + 12R'PO_3H_2 + 24py \rightarrow 3[Fe_7(\mu_3{-}O)_2(RCO_2)_9(R'PO_3)_4(py)_8]X + 18RCO_2H + 7HNO_3 + H_2O \quad (R = Ph, {}^tBu; X = Cl, NO_3\ R' = Ph, {}^tBu) \quad (4)$$

If no pyridine is used, treatment of $[Fe_3(\mu_3\text{-}O)(RCO_2)_6(H_2O)_3]Cl$ in MeCN with 1 equiv of $PhPO_3H_2$

or $C_{10}H_{17}PO_3H_2$ gives nonanuclear clusters $[Fe_9(\mu_3\text{-}O)_2(\mu_2\text{-}OH)(^tBuCO_2)_{10}(PhPO_3)_6\ (H_2O)_5(MeCN)]$ **7** and $[Fe_9(\mu_3\text{-}O)_2(\mu_2\text{-}OH)(PhCO_2)_{10}(C_{10}H_{17}PO_3)_6(H_2O)_6]$ **8** respectively.

$$3[Fe_3(\mu_3{-}O)(RCO_2)_6(H_2O)_3]Cl + 6R'PO_3H_2 \rightarrow [Fe_9(\mu_3{-}O)_2(\mu_2{-}OH)(RCO_2)_{10}(R'PO_3)_6(X)_6] + 8RCO_2H + 3HCl \quad (5)$$

X = $(H_2O)_5(MeCN)$ and $(H_2O)_6$ for **7** and **8** respectively.

We have also explored the use of hydrogen peroxide as a reagent as iron complexes of peroxide have been spectroscopically identified as reaction intermediates for dioxygen-activating diiron proteins[20] or for Gif-type reactivity.[21] The reaction of $[Fe_3(\mu_3\text{-}O)(^tBuCO_2)_6(H_2O)_3]NO_3$ with phosphonic acid (RPO_3H_2) in presence of 30% H_2O_2 yielded peroxo bridged hexanuclear clusters $[Fe_6(\mu_3\text{-}O)_2(O_2)(^tBuCO_2)_8(RPO_3)_2(H_2O)_2]$ (R = Ph, $C_{10}H_{17}$) **9** and **10**. If we use 2−3 drops of pyridine in the similar reaction condition, we obtain another peroxo bridged hexanuclear cluster $[Fe_6(\mu_3\text{-}O)_2(O_2)(^tBuCO_2)_8(^tBuPO_3)_2(py)_2]$ **11** which has the same composition as **9** and **10**, except that terminal H_2O ligands have been replaced by pyridines. Thus the formation can be summarized as:

$$2[Fe_3(\mu_3{-}O)(^tBuCO_2)_6(H_2O)_3]NO_3 + 2RPO_3H_2 + H_2O_2 \rightarrow [Fe_6(\mu_3{-}O)_2(O_2)(^tBuCO_2)_8(RPO_3)_2(X)_2] + 4^tBuCO_2H + 2HNO_3 \quad (X = H_2O \text{ or Py},\ R = Ph, C_{10}H_{17}, {}^tBu) \quad (6)$$

A closely related $\{Fe_6\}$ cage with three bridging peroxides has been reported by Shwecky et al.[22] Finally, with pivalate as the carboxylate, and excluding pyridine entirely, the larger cluster $[Fe_{14}(\mu_3\text{-}O)_4(O_2)_2(^tBuCO_2)_{12}(PhPO_3)_8(H_2O)_{12}](NO_3)_2$ **12** was isolated.

Description of Structures. Molecular Structures of $[Fe_4(\mu_3\text{-}O)Cl(PhCO_2)_3(PhPO_3)_3(py)_5]$ 1 and $[Fe_4(\mu_3\text{-}O)(^tBuCO_2)_4(C_{10}H_{17}PO_3)_3(py)_4]$ 2. The molecular structure of **1** is depicted in Figure 1; **2** has a very similar tetranuclear core and selected bond lengths for the two structures are given in Table 2. In both cages the tetranuclear core contains a $\{Fe_3(\mu_3\text{-}O)\}^{7+}$ triangle similar to that of starting material but where three carboxylates in one face of the triangle have been displaced by three phosphonates. These three phosphonates bind to a single Fe^{III} site, producing a tetrahedron of iron(III) sites. The

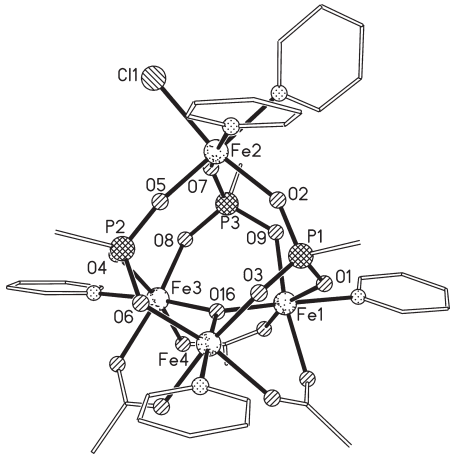

Figure 1. Structure of **1** in the crystal. H-atoms and methyl groups on carboxylate and phosphonates omitted for clarity.

bond lengths between the μ_3-oxide and the three iron centers in the triangle fall in the range 1.93−1.95 Å in **1** and in the range 1.93 to 1.960 Å in **2**. The Fe···Fe distances are close to 3.34 Å and Fe−O−Fe angles very close to 120° in both structures, with the μ_3-oxide essentially within the plane of the Fe_3 triangle. The three iron sites each have a single terminal pyridine attached to them completing their octahedral coordination geometries. On the basis of these structural considerations, the Fe triangle should show magnetic behavior due to an equilateral triangle of spin centers.

The fourth iron site is different in the two structures. In each case it is attached to the $\{Fe_3(\mu_3\text{-}O)\}^{7+}$ unit through three 3.111-bridging phosphonates (Harris notation[23]), but in **1** there are two terminal pyridines and a terminal chloride attached to this site while in **2** there is a single terminal pyridine and a chelating pivalate bound to this apical iron (III) center. The contacts between this apical iron and the three iron sites within the triangle fall in the range 4.74−4.76 Å in **1** and in the range 4.64−4.72 Å in **2**.

Compound **1** crystallizes in the rhombohedral space group *R*3 with two pyridine and two diethyl ether molecules in the lattice per formula unit, while **2** crystallizes in the monoclinic space group $P2_1/c$ with three MeCN molecules as solvents of crystallization.

Molecular Structures of $[Fe_7(\mu_3\text{-}O)_2(PhPO_3)_4(RCO_2)_9(py)_6]$ (R = Me 3, Ph 4) and $[Fe_7(\mu_3\text{-}O)_2(^tBuCO_2)_8(^tBuPO_3)_4(py)_8](NO_3)$ 5. Compounds **3**, **4**, and **5** have very similar structures which are depicted in Figure 2 and selected bond length ranges are listed in Table 2. Compound **3** crystallizes in the triclinic space group $P\bar{1}$, compound **4** in orthorhombic space group $Pca2_1$, whereas **5** crystallizes in monoclinic $P2_1/c$ space group.

The core of complexes **3**−**5** can be described as two equivalent trinuclear oxo-centered $\{Fe_3(\mu_3\text{-}O)\}^{7+}$ units connected via a single iron atom through four phosphonate ligands. The $\{Fe_3(\mu_3\text{-}O)\}^{7+}$ triangle unit is closely related to that of the starting material except that the two carboxylates on one edge of each triangle have been replaced by phosphonates. The presence of different ligands on the edges of the triangle leads to asymmetry in the bonds from the central μ_3-oxide to the Fe sites. In

(20) (a) Kim, K.; Lippard, S. J. *J. Am. Chem. Soc.* **1996**, *118*, 4914. (b) Zhang, X.; Furutachi, H.; Fujinami, S.; Nagatomo, S.; Maeda, Y.; Watanabe, Y.; Kitagawa, T.; Suzuki, M. *J. Am. Chem. Soc.* **2005**, *127*, 826. (c) Moenne-Locoz, P.; Krebs, C.; Herlihy, K.; Thiel, E. C; Huynh, B. H; Loehr, T. M. *Biochemistry*. **1999**, *38*, 5290. (d) Kitazima, N.; Tamura, N.; Amagai, H.; Fukui, H.; Moro-oka, Y.; Mizutani, Y.; Kitagawa, T.; Mathur, R.; Heerwegh, K.; Reed, C. A.; Randall, C. R.; Que, L.; Tatsumi, K. *J. Am. Chem. Soc.* **1994**, *116*, 9071. (e) Dong, Y.; Menge, S.; Brenan, B. A.; Elgren, T. E.; Jang, H. J.; Pearce, L. L.; Que, L.Jr. *J. Am. Chem. Soc.* **1993**, *115*, 1851. (f) Brunold, T. C.; Tamura, N.; Kitazima, N.; Moro-oka, Y.; Solomon, E. I. *J. Am. Chem. Soc.* **1998**, *120*, 5674.

(21) (a) Tapper, A. E.; Long, J. R.; Staples, R. J.; Stavropoulos, P. *Angew. Chem., Int. Ed.* **2000**, *39*, 2343. (b) Kiani, S.; Tapper, A.; Staples, R. J.; Stavropoulos, P. *J. Am. Chem. Soc.* **2000**, *122*, 7503.

(22) Shweky, I.; Pence, L. E.; Papaefthymiou, G. C.; Sessoli, R.; Yun, J. W.; Bino, A.; Lippard, S. J. *J. Am. Chem. Soc.* **1997**, *119*, 1037.

(23) Coxall, R. A.; Harris, S. G.; Henderson, D. K.; Parsons, S.; Tasker, P. A.; Winpenny, R. E. P. *Dalton. Trans.* **2000**, 2349.

Table 2. Selected Bond Ranges (Å) for Compounds **1**−**12** (e.s.ds ca. 0.002 Å)

compound	Fe−O(oxide)	Fe−O(carbox)	Fe−O(phos)	Fe-μ_2-O(phos)	Fe-E(solvent)
1	1.927−1.948	2.032−2.067	1.922−1.990		2.177−2.291[a]
2[b]	1.928−1.961	2.027−2.046	1.889−1.992		2.220−2.243[a]
3[c]	1.859−1.971	1.988−2.060	1.914−1.971		2.194−2.262[a]
4[d]	1.867−1.955	1.999−2.082	1.924−1.979		2.179−2.233[a]
5	1.869−1.947	2.017−2.040	1.938−1.972		2.142−2.265[a]
6	1.887−1.951	1.998−2.059	1.914−1.974		2.187−2.246[a]
7	1.897−1.938	1.980−2.041	1.934−2.035	2.050−2.128	2.238[a] 2.036−2.147[e]
8	1.895−1.939	1.989−2.071	1.917−2.025	2.050−2.160	2.037−2.129[e]
9[f]	1.892−1.905	1.972−2.098	1.963−1.967	2.089−2.098	2.123[e]
10[g]	1.884−1.910	1.971−2.115	1.938−1.979	2.093−2.116	2.095−2.106[e]
11[h]	1.889−1.935	1.978−2.052	1.959−1.984	2.122−2.132	
12[i]	1.873−1.914	1.967−2.056	1.935−1.990	2.065−2.093	2.006−2.090[e]

[a] Solvent pyridine. [b] The molecule also includes a chelating carboxylate with Fe−O bonds of 2.135 and 2.165 Å. [c] The molecule also includes a chelating carboxylate with Fe−O bonds of 2.173 and 2.203 Å. [d] The molecule also includes a chelating carboxylate with Fe−O bonds of 2.125 and 2.152 Å. [e] Solvent = H_2O. [f] The molecule also includes a peroxide with Fe−O bonds between 2.029 and 2.042 Å. [g] The molecule also includes a peroxide with Fe−O bonds between 2.021 and 2.048 Å. [h] The molecule also includes a peroxide with Fe−O bonds between 2.010 and 2.041 Å. [i] The molecule also includes a peroxide with Fe−O bonds between 2.091 and 2.110 Å.

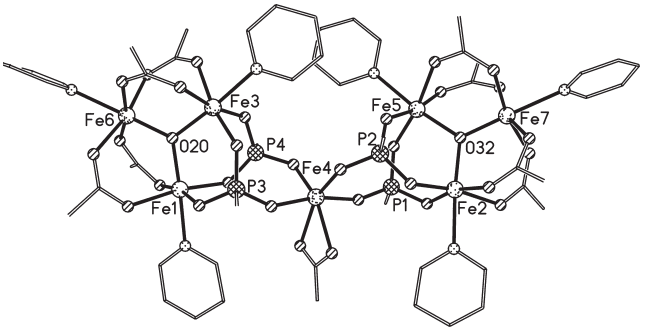

Figure 2. Structure of **3** in the crystal. H-atoms and methyl groups on carboxylate and phosphonates omitted for clarity.

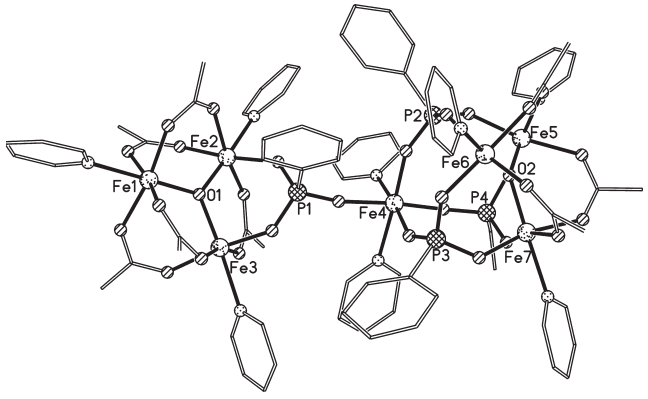

Figure 3. Structure of **6** in the crystal. H-atoms and methyl groups on carboxylate and phosphonates omitted for clarity.

each case the unique Fe site which is not bound to phosphonate ligands forms shorter bonds (1.87 to 1.88 Å) to the bridging oxide, while the Fe-oxide bonds to the other Fe sites within the triangle range from 1.92 to 1.96 Å. In each triangle the oxide lies within the mean plane of the three Fe centers. Clearly the triangles are isosceles rather than equilateral (as in **1** and **2**). All the iron atoms in each $\{Fe_3(\mu_3\text{-}O)\}^{7+}$ triangular units are in distorted FeO_5N coordination environment with terminal pyridine ligands completing the coordination spheres.

The two equivalent triangle units of $\{Fe_3(\mu_3\text{-}O)\}^{7+}$ are linked to the central iron(III) site through bridging phosphonates. The O-donors from phosphonate occupy four of the six coordination sites on this center in **3**−**5**. In **3** and **4** the remaining sites are occupied by two oxygen donors from chelating acetate and benzoate ligands, respectively, giving a distorted FeO_6 octahedral environment with the chief distortion due to the chelating group. In **5** two pyridine molecules are bound to the bridging Fe site, with the pyridines arranged *trans* to one another giving an FeO_4N_2 octahedral environment. The two $\{Fe_3(\mu_3\text{-}O)\}^{7+}$ triangular units in each Fe_7 cage are coplanar. All the four phosphonates exhibit 3.111 binding modes. The Fe···Fe separations within the triangles are in the range of 3.25−3.4 Å with distances over the O−P−O bridges in the range 4.7 to 5.0 Å.

Molecular Structures of $[Fe_7(\mu_3\text{-}O)_2(PhPO_3)_4(MeCO_2)_8(py)_8]$ 6. The molecular structure of **6** is depicted in Figure 3 and selected bond length ranges are listed in Table 2. Compound **6** crystallizes in the space group $P2_1/c$ with five pyridine molecules as solvents of crystallization. The core can be described as a trinuclear oxo-centered $\{Fe_3(\mu_3\text{-}O)\}^{7+}$ unit linked through a phosphonate ligand to a capped $\{Fe_4\}$ tetrahedron unit related to compounds **1** and **2**. The $\{Fe_4\}$ fragment, as in **1** and **2**, contains a $\{Fe_3(\mu_3\text{-}O)\}^{7+}$ unit where three carboxylates from one face have been displaced by phosphonates, with these three phosphonates then binding to the apical iron(III) center [Fe(4)]. Each edge of the triangle within the $\{Fe_4\}$ is therefore bridged in an equivalent manner. Within the isolated $\{Fe_3(\mu_3\text{-}O)\}^{7+}$ triangle a single carboxylate of the starting material has been replaced by a phosphonate ligand; this means that one edge of the triangle is chemically distinct from the other two edges. The phosphonate links the two cages, binding to the apical iron site of the $\{Fe_4\}$ fragment. The four phosphonate ligands therefore all show the 3.111 binding mode. The Fe···Fe contacts within the triangles fall in the range 3.29 to 3.37 Å. The distances between the apical iron and the other Fe sites in the $\{Fe_4\}$ unit are between 4.73 and 4.79 Å. The shortest Fe···Fe contact between the triangle and the Fe_4 is 5.96 Å. The bond lengths involving the two μ_3-oxides are somewhat different; in the $\{Fe_3\}$ triangle the three Fe−O distances fall in the range 1.89 to 1.92 Å, while the distances with the triangle of the $\{Fe_4\}$ moiety are more variable, with one at 1.92 Å and the other two 1.95 Å. In both cases Fe−O−Fe bond angles sum to approximately 360°.

Molecular Structure of $[Fe_9(\mu_3\text{-}O)_2(\mu_2\text{-}OH)(^tBuCO_2)_{10}(PhPO_3)_6(H_2O)_5(MeCN)]$ 7 and $[Fe_9(\mu_3\text{-}O)_2(\mu_2\text{-}OH)(PhCO_2)_{10}(C_{10}H_{17}PO_3)_6(H_2O)_6]$ 8. Compounds **7** and **8** have very similar structures depicted in Figure 4 and selected bond length ranges are listed in Table 2. Compound **7** crystallizes in the monoclinic space group $P2_1/n$, whereas **8** in triclinic space group $P\bar{1}$.

The core structures of **7** and **8** can be described as containing three planes of iron(III) centers. The outer two planes consist of two equivalent trinuclear oxo-centered $\{Fe_3(\mu_3\text{-}O)\}^{7+}$ triangles related to the precursors with one carboxylate from each edge replaced by a phosphonate. The remaining three iron centers are found in the central region, bound O-donors from the six phosphonates, and arranged as a pair of Fe centers bridged by a hydroxide, and a single isolated iron site. There is some resemblance to the $\{Fe_9\}$ citrate "triple-decker" reported by Bino et al.[24] except that in that previous example the three central iron sites form an oxo-centered triangle and the exterior Fe_3 triangles are more irregular.

Each of the pair of hydroxide bridged iron sites is bound to four O-donors from phosphonates, a single oxygen from a carboxylate and the μ-hydroxide. The single Fe(III) site is bound to two oxygens from phosphonates, two from carboxylates and has two terminal water molecules attached. The two carboxylates also form H-bonds to terminal water molecules attached to Fe centers within the oxo-centered triangles. Two of the six phosphonates show the 3.111 binding mode and the remaining four show the 4.211 modes. All the Fe(III) centers are six coordinate and all, except Fe1 in compound **7**, have an octahedral O_6 coordination sphere; Fe1 atom in **7** has a terminal MeCN bound giving an O_5N coordination sphere. The μ_3-oxides lie within the plane of the three iron centers of their respective triangles, and the Fe−O−Fe angles about each of these oxides sum to approximately 360°. The protonation levels of the O^{2-}, OH^-, and H_2O groups were determined from a combination of charge balance considerations, inspection of bond lengths, and BVS calculations.[25] BVS calculations also confirm the +III oxidation state of the Fe atoms.

Molecular Structure of $[Fe_6(\mu_3\text{-}O)_2(O_2)(^tBuCO_2)_8(R\text{-}PO_3)_2(X)_2]$ (R = Ph, $C_{10}H_{17}$, ^{t}Bu, X = H_2O, Py) (9−11). Compounds **9**−**11** have very similar structures and are depicted in Figure 5; selected bond length ranges are given in Table 2. Compound **9** crystallizes in the orthorhombic space group *Pnma*, compounds **10** and **11** in monoclinic space group $P2_1/n$. In each case the crystal lattice contains co-crystallized molecules of MeCN. The structure contains two equivalent trinuclear oxo-centered $\{Fe_3(\mu_3\text{-}O)\}^{7+}$ carboxylate moieties linked in a face-to-face fashion by peroxo- and phosphonate bridges producing a distorted trigonal prism. The peroxide bridge is bound in a 4.22 mode; the only other examples of such binding mode occurs in $[Fe_6(\mu_3\text{-}O)_2(O_2)_3(OAc)_9]^-$ [22] and $[Fe_6(\mu_3\text{-}O)_2(O_2)(RCO_2)_{12}(H_2O)_2]$,[14b] where the O−O distance is in the range of 1.47−1.48 Å. Here these O−O distances are 1.468(2) in **9**, 1.451(7) in **10**, and 1.496(7) in **11**.

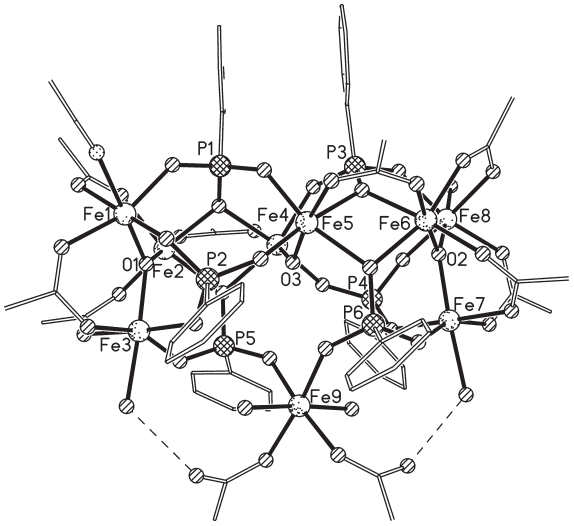

Figure 4. Structure of **7** in the crystal. H-atoms and methyl groups on carboxylate and phosphonates omitted for clarity.

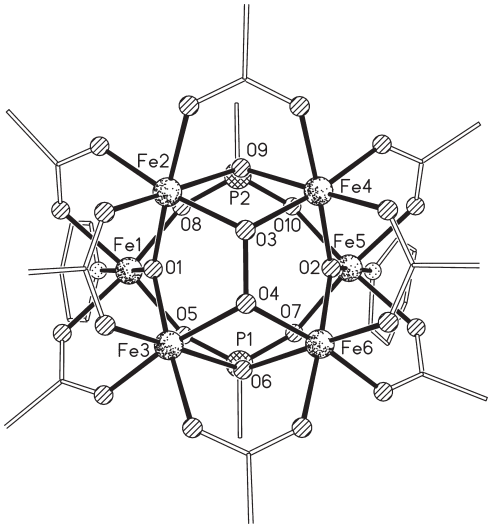

Figure 5. Structure of **9** in the crystal. H-atoms and methyl groups on carboxylate and phosphonates omitted for clarity.

The structure of the triangles is related to the starting material with the three carboxylates on one face replaced by two phosphonate ligands and the peroxo bridge. The μ_3-oxides are planar, and almost all the Fe−O bonds involving these oxides fall in the range 1.88 to 1.91 Å; the exception is the Fe1−O1 contact in **11** which is longer at 1.935(5) Å. The Fe···Fe contacts within each triangle falls into the same pattern, with one short Fe···Fe contact, in the range 3.171 to 3.209 Å, and two longer Fe···Fe contacts, in the range, 3.319 to 3.344 Å, so each triangle is approximately isosceles. The two Fe···Fe contacts within the rectangular face of the trigonal prism that contains the peroxide are in the range 3.133 to 3.186 Å. The final Fe···Fe contact that is an edge of the trigonal prism is much longer in each case, falling in the range 4.90 to 4.93 Å.

Raman bands due to the O−O stretch of the bound peroxide are found 850−860 cm^{-1} for each of compounds **9**−**11**.

Molecular Structure of $[Fe_{14}(\mu_3\text{-}O)_4(O_2)_2(PhPO_3)_8(^tBuCO_2)_{12}(H_2O)_{12}](NO_3)_2$ 12. A labeled representation

(24) Bino, A.; Shweky, I.; Cohen, S.; Bauminger, E. R.; Lippard, S. J. *Inorg. Chem.* **1998**, *37*, 5168.
(25) Liu, W.; Thorp, H. H. *Inorg. Chem.* **1993**, *32*, 4102.

of complex **12** is shown in Figure 6. Selected bond lengths ranges are given in Table 2. Compound **12** crystallizes in the monoclinic space group *Pnn2*. The lattice contains two nitrate anions per dicationic $[Fe_{14}(\mu_3\text{-}O)_4(O_2)_2(PhPO_3)_8(^tBuCO_2)_{12}(H_2O)_{12}]^{2+}$ unit, with six MeCN and four water molecules per cage as solvents of crystallization. The cage lies about a crystallographic inversion center; hence there are seven iron centers in the asymmetric unit. The structure of **12** is related to **3** and **4**, and to **9**−**11**; it could be regarded as a dimer of **3** or **4**, with the linked triangles in those heptanuclear cages stacked on top of one another creating trigonal prisms which are held together by phosphonates or peroxides. Alternatively **12** could be regarded as based on **9**−**11**, with the trigonal prisms linked through two single iron centers. The presence of repeating features between different nuclearity structures suggest that regarding these large clusters as built from smaller cages is not unreasonable.

The trigonal prisms here are very similar to those in **9**−**11**, with two phosphonates bridging in a 4.211 mode on two of the three "rectangular" sides of the prism, and with the binucleating oxygen in each case bound to one Fe(III) ion from each triangle. The third side of the prism is occupied by peroxide bridging in the 4.22 mode. The phosphonates which bridge between the trigonal prisms and the single iron sites adopt the 3.111 mode, as in **3** and **4**, and the coordination geometry of the single Fe site is completed by four molecules of H_2O. The O−O peroxo distance of 1.48(5) Å falls in a similar range to the O−O distances in **9**−**11**.

In both of the $\{Fe_3(\mu_3\text{-}O)\}^{7+}$ triangles in the asymmetric unit one Fe−O bond is slightly shorter (1.87−1.89 Å) than the other Fe−O bonds (ca. 1.91 Å). The Fe−O−Fe bond angles sum to very close to 360° and therefore the units can be regarded as isosceles triangles. All the pivalate groups are bridging the Fe centers in the usual 2.11 mode. The protonation levels of the single oxygen atoms in the structure were determined from a combination of charge balance considerations, inspection of bond lengths, and BVS calculations. The trivalent oxidation state of Fe centers was also confirmed from BVS analysis.[25]

Magnetic Properties. The synthetic work has produced six different families of cage complexes. Variable temperature magnetic susceptibility studies of polycrystalline complexes of members of each family−at least one from each−have been performed over the temperature range 2−300 K, in an applied field of 0.1 T, and the resulting plots of $\chi_M T$ versus T are depicted in Figure 7 (χ_M = molar magnetic susceptibility). Several features are common: in all cases the room temperature value of $\chi_M T$ is lower than would be observed for the relevant number of iron(III) centers if the centers were non-interacting. Thus we find the following: for **1**, 9.5; for **2**, 8.9; for **3**, 13.4; for **4**, 12.9; for **6**, 13.0; for **7**, 16.7; for **9** 7.5; for **10**, 7.4; for **12**, 14.1 cm^3 K mol^{-1}. The calculated values for g = 2.00 are 17.5 cm^3 K mol^{-1} for **1** and **2**; 30.6 cm^3 K mol^{-1} for **3**, **4**, and **6**; 39.4 cm^3 K mol^{-1} for **7**; 26.3 cm^3 K mol^{-1} for **9** and **10**; 61.3 cm^3 K mol^{-1} for **12**. In each case this is due to antiferromagnetic exchange between the S = 5/2 centers, and this is also evident in the fall in $\chi_M T$ with decreasing temperature. Compounds **7** and **12** are too large for the magnetic susceptibility to be modeled using conventional matrix diagonalization techniques; however, we have simulated the variable temperature susceptibility for the other compounds using MAGPACK.[19] In all calculations the g-value was fixed as 2.00 and not used as a variable parameter. The measured values of M versus H for these compounds are reported in Figure 8. The calculated values shown in Figure 8 for compounds **1**−**4**, **6**, **9**, and **10** use the parameters used to fit the $\chi_M T$ versus T data. In Figure 9 we show the low-lying energy states for each calculation as a spin ladder.

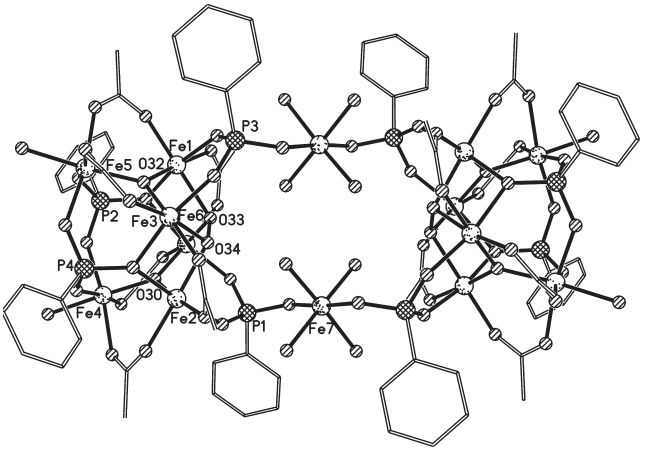

Figure 6. Structure of **12** in the crystal. H-atoms and methyl groups on carboxylate and phosphonates omitted for clarity.

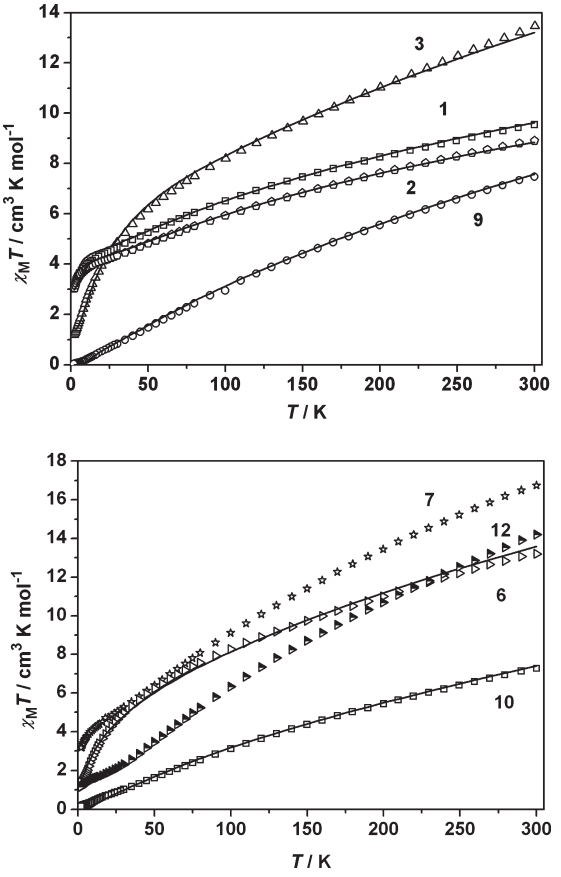

Figure 7. Experimental $\chi_M T$ vs T for compounds **1**−**3**, **6**, **7**, **9**, **10**, and **12** with calculated curves shown for compounds **1**−**3**, **6**, **9**, and **10**.

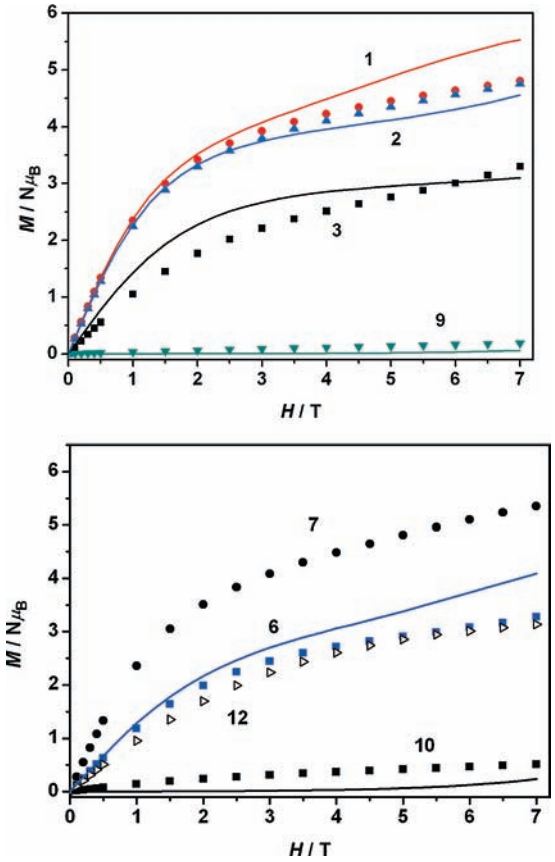

Figure 8. Experimental M vs H for compounds **1**−**3**, **6**, **7**, **9**, **10**, and **12** with calculated curves shown for compounds **1**−**3**, **6**, **9**, and **10**; the calculated curves use parameters used to fit $\chi_M T$ vs T data.

The $\{Fe_4^{III}\}$ compounds **1** and **2** can be viewed as an equilateral triangle of Fe^{3+} centers capped by a fourth iron atom, which means that only two exchange pathways are required in the model (Figure 10). These are as follows: (a) exchange interactions, J_1, between the iron centers within the triangle, mediated via a combination of μ_3-oxide and a single carboxylate and a single phosphonate, and (b) exchange interactions, J_2, between the capped iron center (S_4) and iron atoms in $\{Fe_3O\}$ triangular core mediated through phosphonates. Thus, the data were fitted with a spin Hamiltonian:

$$H = -2J_1[S_1S_3 + S_1S_4 + S_3S_4] - 2J_2S_2[S_1 + S_3 + S_4] \quad (7)$$

The data were simulated (solid line in Figure 7) with parameters $J_1 = -19.3$ and $J_2 = -0.8$ cm^{-1} for **1** and $J_1 = -21.7$ and $J_2 = -1.3$ cm^{-1} for **2**. Analysis of the spin energy levels indicates that $S_T = 2$ spin state is lowest in energy; the first excited state in both cases has $S_T = 3$, with the energy gap to this first excited state being 4.8 cm^{-1} for **1** and 7.8 cm^{-1} for **2** (Figure 9). A simple explanation for the low-lying energy levels comes from considering that the coupling within the equilateral triangle is much larger than the coupling between triangle and capping iron; this gives an $S = 1/2$ ground state for the triangle, and this is coupled weakly to the cap, giving two

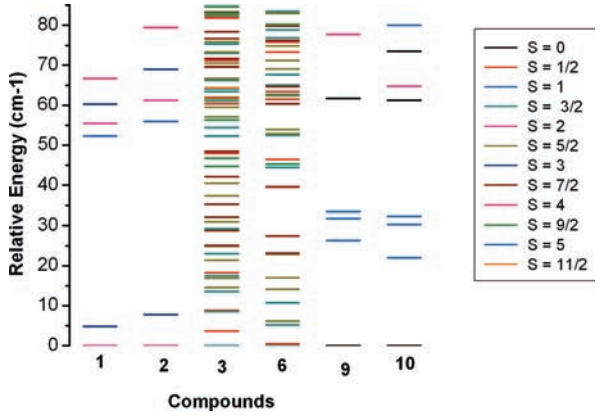

Figure 9. Spin ladders for compounds **1**−**3**, **6**, **9**, and **10**.

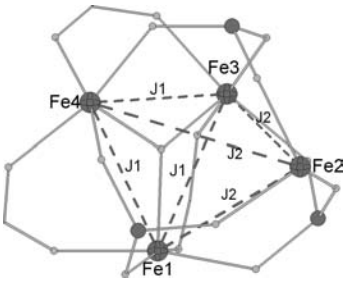

Figure 10. Coupling scheme used to model the magnetic behavior of **1** and **2**.

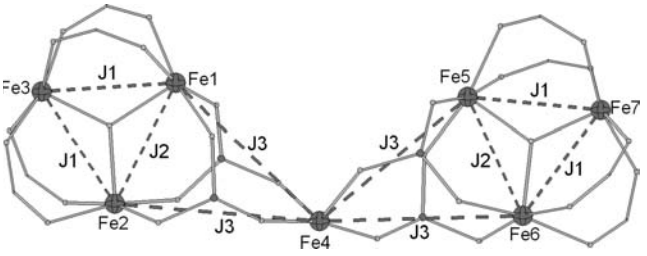

Figure 11. Coupling scheme used to model the magnetic behavior of **3** and **4**.

spin states, $S_T = 2$ and $S_T = 3$. As the exchange via the phosphonates is antiferromagnetic, the $S_T = 2$ state is the lower in energy. To confirm this picture, isothermic variable-field (H) magnetization (M) data were collected in the 1−7 T ranges. The values of magnetization (M/Nμ_B) at the highest field and 2 K temperature are ∼ 4.8 (for **1**) and 4.76 (for **2**), which are intermediate between those expected for $S = 2$ and $S = 3$, suggesting that both states are occupied at low T and high field (Figure 8).

Complexes **3** and **4** consist of two oxo-centered $\{Fe_3(\mu_3\text{-}O)\}^{7+}$ units connected by a central Fe(III) ion through four phosphonates. Within each $\{Fe_3(\mu_3\text{-}O)\}^{7+}$ unit, the iron atoms on two edges are bridged by carboxylate groups while on the third edge by phosphonate bridges. Such differences may reflect in the coupling constants. Therefore three exchange interactions were used in the model (Figure 11): (a) the exchange interaction through the μ_3-O and two carboxylate bridges is represented as J_1, (b) while that through both μ_3-O and two phosphonate bridges as J_2 and (c) the exchange

interaction (J_3) between central Fe^{III} and four Fe^{III} centers in the $\{Fe_3(\mu_3\text{-O})\}$ cores via O−P−O bridges. The Heisenberg spin Hamiltonian for such a model is

$$H = -2J_1[S_1S_3 + S_2S_3 + S_5S_7 + S_6S_7] - 2J_2[S_1S_2 + S_5S_6] - 2J_3S_4[S_1 + S_2 + S_5 + S_6] \quad (8)$$

The data were simulated (solid line Figure 7) with $J_1 = -27.4$, $J_2 = -18.7$, and $J_3 = -0.8$ cm^{-1} for **3**; $J_1 = -28.5$, $J_2 = -18.7$, and $J_3 = -0.8$ cm^{-1} for **4**. We were unable to fit the data with $J_1 = J_2$. Analysis of the spin energy levels indicates that the ground state has $S_T = 3/2$. As in **1** and **2**, exchange within the oxo-centered triangles is stronger than exchange via phosphonates; the ratio of J_1/J_2 will give an $S = 1/2$ state as the lowest energy state for each triangle, and antiferromagnetic exchange between each $S = 1/2$ and the $S = 5/2$ on the Fe center in the link will give the ground state observed (Figure 9). M versus H data of **3** were collected in the 1−7 T range (Figure 8). The value at the highest field and 2 K temperature is $\sim 3.4\ \mu_B$, but the value has not saturated. This is a little above the value expected for an $S = 3/2$ spin state indicating population of the excited $S = 5/2$ state with increasing field.

Complex **6** consists of one oxo-centered $\{Fe_3(\mu_3\text{-O})\}^{7+}$ unit and one $\{Fe_4^{III}\}$ tetrahedron unit similar to that found in complexes **1** and **2** with the two units connected via phosphonates (O−P−O). Within the $\{Fe_3(\mu_3\text{-O})\}^{7+}$ unit, the iron atoms are bridged by carboxylate groups along with μ_3-oxo group. One edge (involving Fe5 and Fe6) is also bridged by a phosphonate; therefore it is likely that this unit should be modeled as an isosceles triangle. The Fe(III) centers in the $\{Fe_3(\mu_3\text{-O})\}^{7+}$ triangular unit of $\{Fe_4^{III}\}$ are connected by combinations of μ_3-oxo, carboxylate, and phosphonate groups; as each edge of the triangle is chemically equivalent we have modeled it as an equilateral triangle. Therefore, the model (Figure 12) used to fit the data includes four exchange interactions: (a) the exchange interaction through both μ_3-O and two carboxylate bridges, J_1, in the isosceles triangle; (b) the exchange through the μ_3-O, carboxylate and phosphonate in the isosceles triangle, J_2; (c) through both μ_3-O, a single carboxylate and a single phosphonate (O−P−O) bridge, J_3 and (d) the exchange between Fe^{III} centers via O−P−O bridges, J_4. The spin Hamiltonian used is

$$H = -2J_1[S_1S_2 + S_1S_3] - 2J_2S_2S_3 - 2J_3[S_5S_6 + S_5S_7 + S_6S_7] - 2J_4S_4[S_2 + S_3 + S_5 + S_6 + S_7] \quad (9)$$

It is impossible to fit the data if $J_1 = J_2$. The temperature dependence of magnetic susceptibility data were simulated (solid line Figure 7) with parameters $J_1 = -25.2$, $J_2 = -17.3$, $J_3 = -23.0$, and $J_4 = -1.08$ cm^{-1}. The resulting spin ladder shows an $S = 3/2$ ground state, with an $S = 1/2$ first excited state 0.5 cm^{-1} higher in energy (Figure 9). The second excited state has $S = 5/2$ and is 14.6 cm^{-1} above the ground state. The calculation of M versus H does not fit perfectly with the measured data (Figure 8), with the calculated magnetization increasing more rapidly than the measured values. This is possibly because we have neglected anisotropy or because our model, even with four exchange interactions, is not sufficient. Introducing still further parameters does not seem justified.

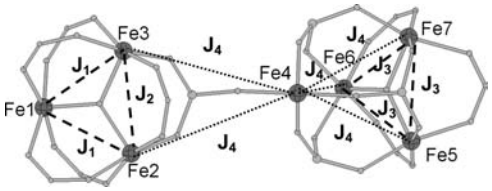

Figure 12. Coupling scheme used to model the magnetic behavior of **6**.

For **7**, the $\chi_M T$ at 300 K is less than the value calculated for nine non-interacting Fe^{III} ions with $g = 2.00$. This value decreases to 3.2 cm^3 K mol^{-1} at 2 K (Figure 7). The low temperature values of $\chi_M T$ indicate that the complex **7** has a non-diamagnetic ground state. Magnetization isotherms were measured at 2 and 4 K in fields up to 7 T and from the experimental data, $M/N\mu_B = 5.2$ at 2 K and 7 T and appears to be approaching saturation (Figure 8), which is consistent with an $S = 5/2$ ground state, or possibly with an $S = 3/2$ ground state with a low-lying $S = 5/2$ excited state. Unfortunately an $\{Fe_9\}$ cluster with low-symmetry is too large to be treated by matrix-diagonalization methods, but we can understand why the lowest energy levels might have these spin values. The structure (Figure 4) contains two oxo-centered triangles, and these would be expected to have $S = 1/2$ spin states as the lowest in energy. There is also a Fe_2 dinuclear fragment bridged by a hydroxide; this is likely to have an $S = 0$ state as the lowest in energy. Third there is an isolated Fe center, with spin $S = 5/2$. As the dinuclear unit is diamagnetic at low temperature, the lowest energy states are similar to those in **3** and **4** because of weak exchange between the $S = 5/2$ spin on the single Fe center and the $S = 1/2$ states of the two triangles.

The room temperature (300 K) $\chi_M T$ values of **9** and **10** are lower than that expected for six non-interacting Fe^{III} ions, and $\chi_M T$ falls to a value approaching zero at 2 K, suggesting an $S_T = 0$ ground state. On the basis of the possible superexchange paths and Fe−O−Fe angles and Fe···Fe separations, a model was developed (Figure 12) which involves three exchange interactions: (a) J_1 between the iron centers in each triangle mediated via a μ_3-O, a single carboxylate and a single phosphonate(O−P−O) bridges, (b) J_2 between the iron centers in each triangle via the μ_3-O, a carboxylate and a peroxo bridge, and (c) J_3 along the edges of the rectangular faces of the trigonal prism, mediated by a μ_2-O (phosphonate), μ_2-O (peroxo) and a carboxylate bridge. The spin Hamiltonian used is

$$H = -2J_1[S_1S_2 + S_1S_3 + S_4S_5 + S_4S_6] - 2J_2[S_2S_3 + S_5S_6] - 2J_3[S_2S_5 + S_3S_6] \quad (10)$$

The best simulation of $\chi_M T$ of **9** and **10** (solid line in Figure 7) was achieved with parameters: $J_1 = -33.5$, $J_2 = -26.0$, and $J_3 = -4.5$ cm^{-1} for **9**; $J_1 = -35.0$, $J_2 = -26.5$, and $J_3 = -3.5$ cm^{-1} for **10**. These parameters result in an $S_T = 0$ ground state separated by around 26 cm^{-1} from the first excited state with $S_T = 1$ (Figure 9). We also examined a model where a fourth interaction, J_4,

was included which was also mediated by the peroxide (Figure 13), however, the best simulation of the data was found with $J_4 = 0$. Magnetization measurements at 2 K confirmed the singlet ground state (Figure 8); however, they also suggest that **10** may contain a small amount of paramagnetic impurities. Complex **11** is expected to have magnetic properties very similar to those of **9** and **10**.

Previous studies of an $\{Fe_6\}$ cage,[22] where two oxo-centered triangles were bridged by three peroxides to form a trigonal prism, were complicated by the presence of a second iron(III) cage in the crystal lattice. Two independent sets of parameters could be used to fit the magnetic data in this case;[22] these two models, expressed using our Hamiltonian, eq 10, would give $J_1 = -51.3$, $J_2 = -33.5$, and $J_3 = 0.8$ cm^{-1} or $J_1 = -47.3$, $J_2 = -31.9$, $J_3 = 0$, and $J_4 = -0.8$ cm^{-1}.

The room temperature (300 K) $\chi_M T$ value of $\{Fe_{14}\}$ **12** is lower than that expected for fourteen non-interacting Fe^{III} ions (Figure 7), and the value gradually decreases to 1.2 cm^3 K mol^{-1} at 2 K. The M versus H measurement does not lead to saturation of magnetization even to 7 T (Figure 8), with a steady increase with field, reaching a value of 3.0 $N\mu_B$ at 2 K. These measurements are consistent with a low-spin, probably $S = 0$ ground state and population of Zeeman components of low-lying $S > 0$ excited states. An $\{Fe_{14}\}$ cluster with very low-symmetry is too large to be computed by matrix-diagonalization methods, but we can perhaps predict $S = 0$ as although the heptanuclear cages **3** and **4** have $S_T = 3/2$ ground states, dimerization of this cage to give the $\{Fe_{14}\}$ cage is probably accompanied by AF-exchange between the two $\{Fe_7\}$ fragments.

Two magnetostructural correlations have been reported for Fe cage complexes. The first, proposed by Gorun and Lippard, is an empirical correlation[14a] between J (cm^{-1}) and the parameter P (Å), which is the shortest superexchange pathway defined as the shortest distance between the metal(s) and the bridging ligand(s), for pairs of doubly or triply bridged high-spin Fe^{III} centers

$$-J = 8.763 \times 10^{11} \exp(-12.663P)$$

The second correlation, proposed more recently by Weihe and Gudel[15a] and refined by the Christou group[15b] is

$$-J = 2 \times 10^{-7}(0.2 - \cos\varphi + \cos^2\varphi) \exp(-7r)$$

This relationship correlates the coupling constant (J) with the Fe−O−Fe angle (φ) at any bridging oxide or hydroxide and the shortest Fe−O distance (r) for interactions between pairs of Fe^{III} centers bridged by oxo, hydroxo, and alkoxo ligands in Fe_n complexes of nuclearity greater than two. In Table 3 the values used in simulation magnetic data are compared to values calculated using these two correlations. The first observation is that both correlations predict the exchange interactions well; the Weihe−Gudel correlation predicts slightly higher exchange couplings than the Gorun−Lippard correlation. In seven cases the values from our simulations lie between the two predictions, and in five cases slightly lower than the Gorun−Lippard prediction. In one case the simulated value is higher than that predicted by Weihe−Gudel. The only cases were the values from the simulations do not match the magnetostructural correlation is J_2 for compounds **9** and **10**. This is the exchange interaction which involves coupling through the side-on peroxide bridge, and the value used in the simulation is approximately twice that predicted. This implies that the peroxide bridge makes a significant contribution to the AF-exchange in this bonding mode leading to a failure of the magnetostructural correlations.

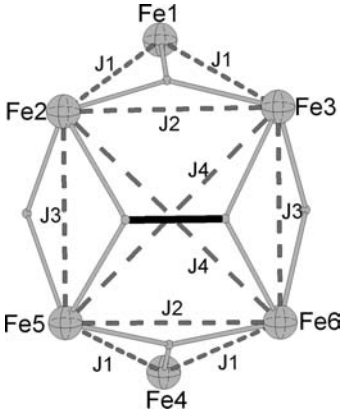

Figure 13. Coupling scheme used to model the magnetic behavior of **9** and **10**.

Conclusions

New tetra-, hexa-, hepta-, ennea-, and tetradeca-nuclear ferric complexes have been made by reacting oxo-centered carboxylate triangles with phosphonates, again showing the power of this approach to the synthesis of new cage complexes. The ability to synthesize cages with similar Fe cores with different phosphonates and carboxylates implies that control of structure is not achieved chiefly by the choice

Table 3. Exchange Coupling Constants[a] and Comparison with Magnetostructural Correlation[b]

complex	J_1 cm^{-1}	J_a cm^{-1}	J_b cm^{-1}	J_2 cm^{-1}	J_a, cm^{-1}	J_b cm^{-1}	J_3 cm^{-1}	J_a cm^{-1}	J_b cm^{-1}
Fe_4 **1**	−19.3	−19.65	−22.6	−0.8[c]					
Fe_4 **2**	−21.7	−18.3	−22.5	−1.3[c]					
Fe_7 **3**	−27.4	−26.1	−28.5	−18.7	−15.2	−20.5	−0.8[c]		
Fe_7 **4**	−28.5	−31.1	−31.4	−18.7	−19.1	−23.8	−0.8[c]		
Fe_7 **6**[d]	−25.2	−30.1	−31.1	−17.3	−24.7	−28.2	−23.0	−19.2	−24.2
Fe_6 **9**	−33.5	−32.1	−35.5	−26.0	−12.9	−15.1	−4.5	−4.1	−4.3
Fe_6 **10**	−35.0	−33.1	−35.3	−26.5	−13.1	−16.5	−3.5	−3.5	−3.9

[a] J_1, J_2, J_3 are derived from the simulation of data, as described in the text. [b] J_a: Lippard−Gorun correlation (ref 14); J_b: Weihe−Gudel correlation (ref 15). [c] Exchange through three atom O−P−O bridge and hence the correlations are not relevant. [d] Also includes a fourth exchange term through phosphonate bridges.

of substitutent in the ligand. The specific reaction conditions are also vital, and here the presence/absence of pyridine and/or hydrogen peroxide is clearly important.

The magnetic exchange interactions in these cages are all antiferromagnetic and consistent with two magnetostructural correlations proposed for Fe dimers and cage complexes. The study also confirms that phosphonate itself is a weak magnetic coupler, while peroxide seems to provide a significant superexchange path between Fe centers in compounds **9** and **10**.

Acknowledgment. We thank the EPSRC (U.K) and the EC-NE "MAGMANet" for funding

Supporting Information Available: Crystallographic data in CIF file format. This material is available free of charge via the Internet at http://pubs.acs.org.